This is pre-published version.
This is accepted manuscript of an article published by Elesiver in Sensors and Actuators: A physical.
Available online https://doi.org/10.1016/j.sna.2021.113083

FEA-based optimization and experimental verification of a typical flexure-based constant force module

Bingxiao Ding[1,2] Xuan Li[*1], Yangmin Li[*2]

[1] School of Physics and Electromechanical Engineering, Jishou University, Jishou 416000, China;
[2] Department of Industrial and Systems Engineering, The Hong Kong Polytechnic University, Hong Kong 999077, China;
[*] Corresponding author: Xuan Li, li_xuan0118@hotmail.com; Yangmin Li, yangmin.li@polyu.edu.hk.

Abstract
To solve the problem of insufficient constant-force stroke of the compliant constant force mechanism (CFM), a FEA-based optimization method based on structural parameters is proposed in this paper. Firstly, a flexure-based constant force module (FBCFM) combined with a Z-shaped beam and a bi-stable beam is designed. By analyzing the force-displacement relationship of the two kind beams, the architectural parameters related to the constant force characteristic of the FBCFM are derived. Then, the initial constant-force stroke with 2.2 mm and output constant force with 13.8 N of the FBCFM are obtained by experimental studies. Furthermore, to explore the parametric effects for the designed FBCFM, parametric evaluation is conducted via MATLAB. Finally, the optimal solution set of architecture parameters is obtained with FEA-based optimization method. Through experimental verification, the constant-force stroke of the optimized FBCFM is 4.5 mm with constant force 8.5 N. The optimization results show the effectiveness and feasibility of the proposed FEA-based optimization method.

Keywords
Constant force compliant mechanism, Z-shaped beam, Bi-stable beam, FEA-based optimization

1. Introduction

A CFM provides a nearly constant output force in a range of input displacements [1-4]. Owing to this adjustable force property, CFM has drawn widely attention from several applications, such as micro-gripper design, ultra-precision polishing and bio-micromanipulation tools [5-8]. For example, the use of CFM to design micro-grippers can be adopted to grasp soft/fragile objects that are sensitive to contact force [9,10]. Traditional electromechanical systems used to manipulate force-sensitive objects are usually equipped with a series of sensors. By using a feedback control algorithm, the contact force can be maintained at a specific value [11,12]. However, the precise sensory apparatus may be failure in harsh industrial environments or not inappropriate equipped in small scale grippers. Furthermore, the feedback controller is more complicated for flexure-based mechanism in order to maintain a constant force [13]. To reduce the dependency on complex control algorithms and complicated

parameter tuning processes, an alternative method based on CFM has been recently proposed from the viewpoint of mechanism design [14-16].

The compliant mechanism utilizes elastic deformation of the flexible element to realize force transmission and movement, which exhibits the advantages of no assembly, no backlash and high movement accuracy [17-20]. For example, to reduce the damage to the fruit during the grasping process, Miao et al. designed a CFM end-effector which is used for picking robots with 8.03N average constant griping force and 95.3% successful rate [21]. To achieve smooth contact with unknown objects, Meaders et al. optimized a near-constant force springs subject to mating uncertainty [22]. Ma et al. presented a large-stroke compliant CFM. Based on the non-dimensionalized metrics, its maximum operational displacement can be obtained at β = 64.5deg. The effectiveness of the non-dimensionalized metrics was demonstrated in comparison of several prototypes [23]. Liu et al. designed a compliant constant force system, which has high stability and can reduce certain external load interference [24]. Wang et al. designed a constant-force bi-stable micro-mechanism, which can exhibit a constant output force of nearly 500N in a displacement range of 50 mm [25]. Tolman et al. designed a compliant CFM, which can achieve large constant-force stroke by optimization of parameters [26]. Chen et al. presented an adjustable constant force mechanism, which can exhibit a constant-force region that is more than 70% of the entire input displacement [27].

The above research shows that CFMs are widely adopted in various applications for their inherent advantages. However, the limited constant-force range has become a bottleneck for their further application. To solve this problem, it is urgent to optimize the constant force property of the CFM. During the literature review, most of optimization methods are complicated. For example, the coding process of particle swarm optimization (PSO) is complicated, and it exhibits disadvantages such as being easy to fall into local optimal and unable to effectively solve combinatorial optimization [28]. The FEA-based optimization has fewer applications, but its implementation process is easy to access and exhibits the advantages of strong versatility, response surface analysis, finding the sensitivity of parameters, and recommending the best combination of parameters, etc [29].

Overall, the main contribution of this work is optimization of constant force property of a proposed FBCFM based on FEA-based optimization. Firstly, design and modeling of the FBCFM based on the parallel structure of the Z-shaped beam and the bi-stable beam is presented in Section 2. Secondly, parametric evaluation of the FBCFM is conducted with MATLAB in Section 3. In addition, constant force property of the FBCFM is optimized with FEA-based optimization in Section 4. Furthermore, experimental studies are performed in Section 5. Finally, a conclusion is summarized in Section 6.

2. Module design and modeling

Different from the traditional mechanism, the CFM does not obey Hooke's law and can be obtained by the combination of positive-stiffness and negative-stiffness mechanisms. At present, flexible straight beams are often utilized as positive-stiffness beams.

However, there is a stress hardening phenomenon in that mechanism, that is, as the input displacement increases, its stiffness will increase. In turn, the increase in tensile stress leads to an increase in bending stiffness. In addition, the force-displacement of the flexible straight beam is non-linear, which means it cannot make full use of the negative-stiffness region of bi-stable beam. To compensate the shortcomings of these drawbacks, a Z-shaped beam is designed as a positive-stiffness mechanism, and the force-displacement properties are shown in Fig. 1. It can be seen that as the input displacement increases, the Z-shaped beam exhibits better linear force-displacement properties than flexible straight beams, and can provide a larger stroke to neutralize the negative stiffness to perform constant force property.

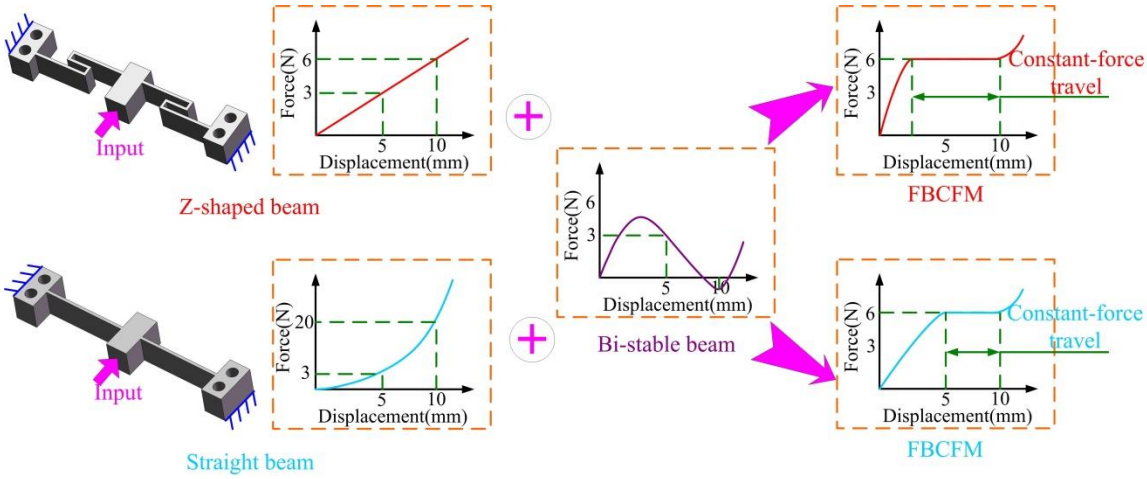

Fig. 1 Comparison of force-displacement property of two flexible beams

2.1. Module design

To make the modeling and optimization method more typical and universal, a representative FBCFM module combining with Z-shaped beam and bi-stable beam is designed. The CAD model of the FBCFM is shown in Fig. 2, which adopts the principle of positive and negative stiffness matching to obtain constant force output property [30]. The overall structure is composed of two Z-shaped beams and four bi-stable beams. To improve the overall rigidity and compactness of the mechanism, each side is composed of two bi-stable beams in parallel. Owing to the buckling property of the bi-stable beam [31], the FBCFM can exhibit zero stiffness in a certain displacement range.

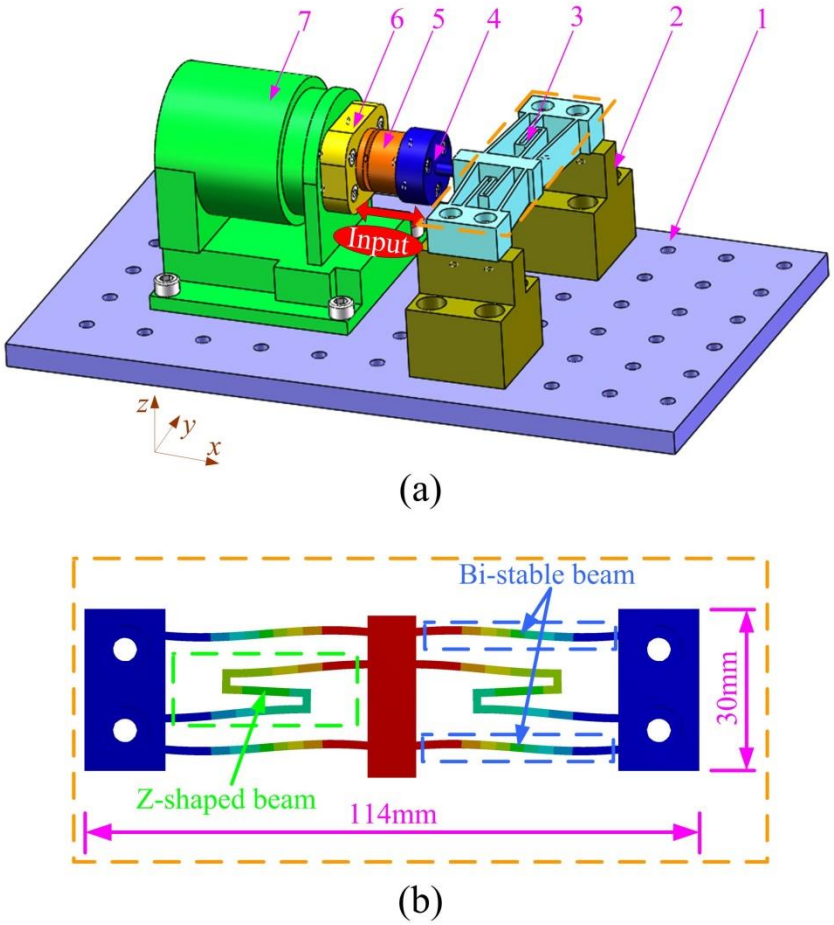

Fig. 2 CAD model for the FBCFM. (a) Assembly : 1-anti-vibration stage, 2-support base, 3-FBCFM, 4-connector 1, 5-force sensor, 6-connector 2, 7-voice coil motor. (b) FBCFM schematic

2.2. Analysis of positive stiffness

By analyzing the force-displacement relationship of the negative/positive stiffness beams, the relevant architecture parameters that affect its mechanical properties can be obtained. The Z-shaped beam of the FBCFM is composed of three flexible leaf beams and two connecting beams, as shown in Fig. 3. In this figure, where F_1 is applied force, l_1, l_2, and l_3 are the length of each leaf beam, θ_1, θ_2, and θ_3 are the deformation angle of each leaf beam, t is the thickness of the Z-shaped beam, b is the width of the Z-shaped beam, and M_1 is the moment of the fixed end of the Z-shaped beam.

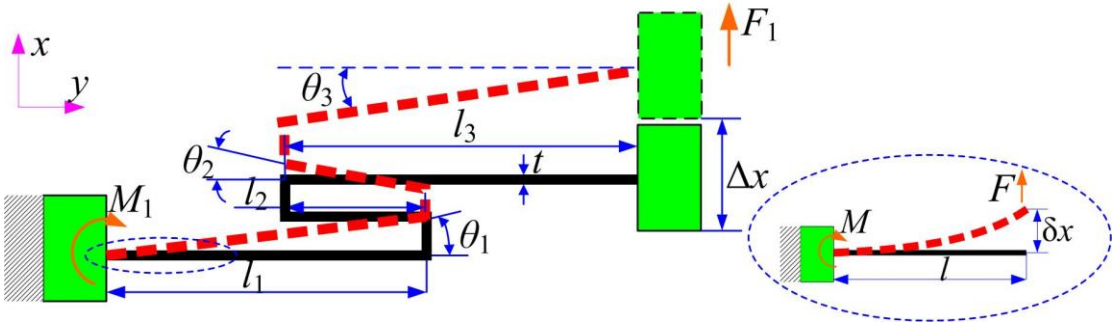

Fig. 3 Deformation diagram of Z-shaped beam for force

For a cantilevered leaf beam, when the cantilever end is subjected to a force F, the following equations can be derived as:

$$\frac{Fl^2}{2EI}-\frac{Ml}{EI}=0 \tag{1}$$

$$\frac{Fl^3}{3EI}-\frac{Ml^2}{2EI}=\delta x \tag{2}$$

where δx is the output displacement of the free end, M is the moment of the fixed end of the leaf beam, l is the length of the leaf beam, E is the Young's modulus, and I denote the inertia moment. According to the Eq. (1) and (2), the following equation can be obtained:

$$\delta x=\frac{Fl^3}{12EI} \tag{3}$$

Because the Z-shaped beam is composed of three blade beams, the output force is:

$$F_1=\sum_{i=1}^{3}F_{\theta_i} \tag{4}$$

where $F_{\theta i}$ is the output force of a single leaf beam in the Z-shaped beam. According to Eq. (1), (2) and (3), the following equation can be expressed:

$$F_{\theta_i}=\frac{7EI\theta_i}{l_i^2} \tag{5}$$

According to the geometric relationship of the Z-shaped beam, the following equation is derived as:

$$\begin{cases} l_1\left(1-\cos\theta_1\right)-l_2\left(1-\cos\theta_2\right)+l_3\left(1-\cos\theta_3\right)=0 \\ l_1\sin\theta_1+l_2\sin\theta_2+l_3\sin\theta_3=\Delta x \\ \theta_1=\theta_3 \end{cases} \tag{6}$$

Through the above analysis, it can be obtained that the length and width of the connecting beam have no obvious influence on the positive-stiffness characteristics of the Z-shaped beam. To reduce the workload of calculation, the above parameters were not selected to participate in process of FEA-based optimization.

2.3. Analysis of negative stiffness

The negative-stiffness structure adopts a bi-stable beam with buckling properties, and its modeling is shown in Fig. 4. The buckling deformation will be induced when the bi-stable beam is subjected to the force F_2. Referring to this figure, L and t are the length and width of the bi-stable beam, θ is the inclination angle of the beam relative to the plane which is relatively vertical to fixed plane, and ε is the output displacement of the bi-stable beam for F_2.

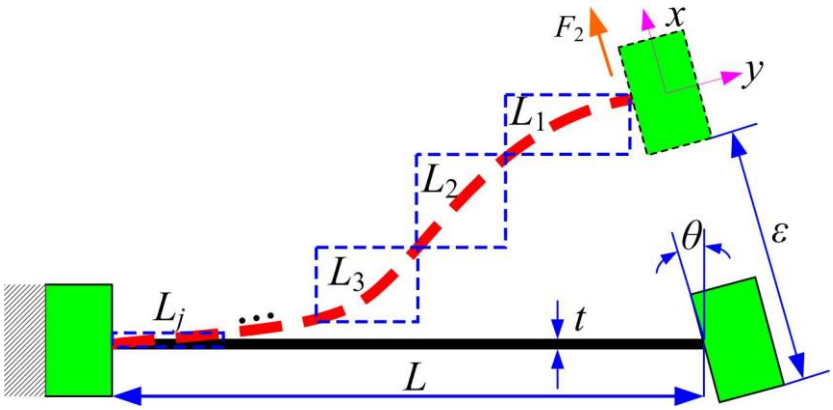

Fig. 4 Modeling of bi-stable beam

To improve the reliability of calculation, the bi-stable beam can be divided into countless extremely small elements (critical point). According to the reference [32], the buckling force at the j-th critical point of the bi-stable beam can be derived as:

$$F_j = \frac{4EI_d\lambda_j^2}{L_j^2} \tag{7}$$

where E is the Young's modulus, $I_d = bt^3/12$ is the inertia moment of the bi-stable beam, and L_j is the length of the short section at the j-th critical point of the beam, $\lambda_j = \pi, 4.493, 2\pi \ldots, j = 1, 2, 3 \ldots$. The negative-stiffness expression of a bi-stable beam can be derived as:

$$k_n \approx \frac{33EI_d}{L^3} \tag{8}$$

According to Eq. (7) and (8), the force-displacement expression can be derived as:

$$F_2 = ES\frac{\varepsilon}{L}\left(\frac{\varepsilon}{L} - \sin\theta\right)\left(\frac{\varepsilon}{L} - 2\sin\theta\right) \tag{9}$$

where $S = bt$ is the cross-sectional area of the beam. When θ is zero, the force-displacement relationship of conventional straight beam can be derived using Eq. (9). According to Eq. (4) and (9), the force-displacement expression of the FBCFM can be obtained.

$$F = \sum_{i=1}^{3} F_{\theta_i} + ES\frac{\varepsilon}{L}\left(\frac{\varepsilon}{L} - \sin\theta\right)\left(\frac{\varepsilon}{L} - 2\sin\theta\right) \tag{10}$$

2.4. Constant force property verification

To verify the correctness of the theoretical analysis, experimental studies are conducted in this subsection. The adopted material for the FBCFM is PLA-ST which has high flexibility with density 1250 kg/m^3, Young's modulus E = 1.477 GPa, Poisson's ratio μ = 0.3. The main architectural parameters of the FBCFM are listed in Table I. Among them, t_z and t_b are the width of the Z-shaped beam and the bi-stable beam, respectively.

Table I Main architectural parameters of FBCFM

Main architectural parameters of FBCFM								
parameters	l_1	l_2	l_3	t_z	L	θ	t_b	b
values	25.5mm	13.5mm	25.5mm	1.0mm	37.87mm	8°	1.0mm	15.0mm

Through collecting the displacement-force data of the FBCFM by experimental setup, the comparison of theoretical and experimental force-displacement results are shown in Fig. 5. Referring to this Figure, the theoretical and experimental results are relatively consistent, with 2.2 mm constant travel range. The experimental curve starts to become flat at the input displacement of about 2.45 mm, the constant force is approximately 13.8 N, and the constant-force variation range is approximately [13.7, 13.9] N. The input displacement interval corresponding to the constant force is about [2.45, 4.65] mm, which means that the positive and negative stiffness of the FBCFM begin to cancel each other out in this displacement interval, and the FBCFM tends to zero stiffness. The main reason for the error is summarized as the difference in the filling density and printing method of 3D printer, the reduced capability of elastic recovery of the mechanism in the repeated test and difference of the bolts pre-tightening force in the setup of the experimental system.

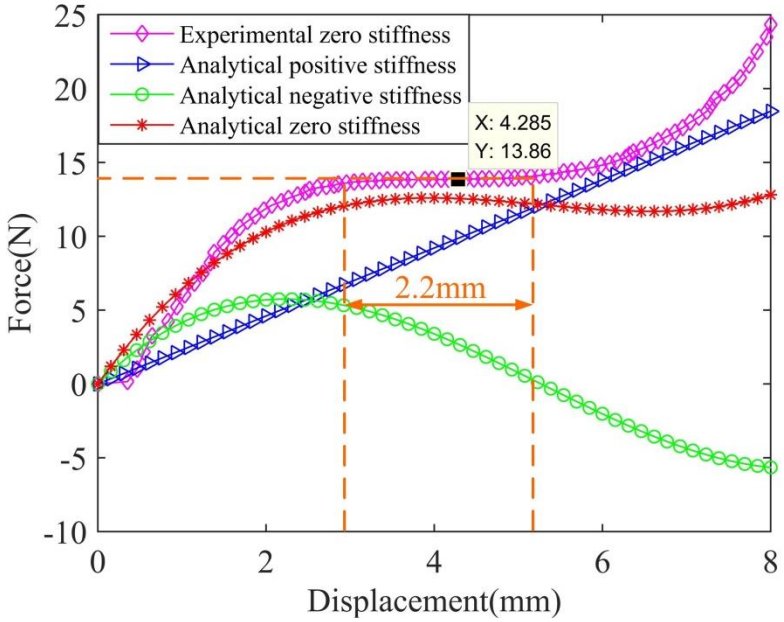

Fig. 5 Comparison of constant-force results

3. Parametric evaluation

Referring to equation (10) and Table I, it can be seen that the constant force property of the FBCFM are mainly affected by the structural parameters of the Z-shaped beam and the bi-stable beam. Therefore, it is necessary to explore the influence of some architecture parameters on the force-displacement property of the FBCFM.

When analyzing the influence of a certain parameter on the constant force property, other parameters should remain constant. When the selected parameters of the Z-shaped beam l_2 and t_z change, the force-displacement property of the FBCFM is

shown in Fig. 6. When the selected parameters of bi-stable beam θ and t_b change, the force-displacement property of the FBCFM is shown in Fig. 7.

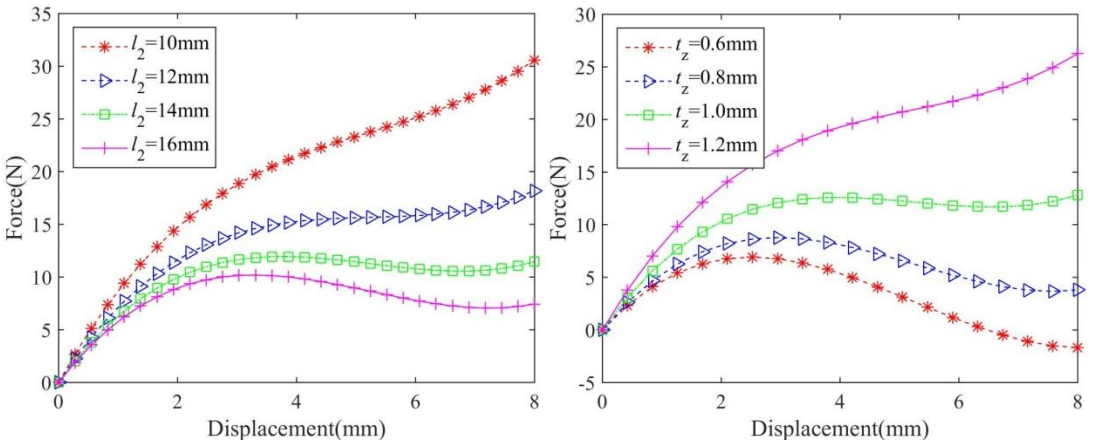

(a) (b)

Fig. 6 The influence of l_2, t_z on the constant force properties of the FBCFM (a) l_2, (b) t_z

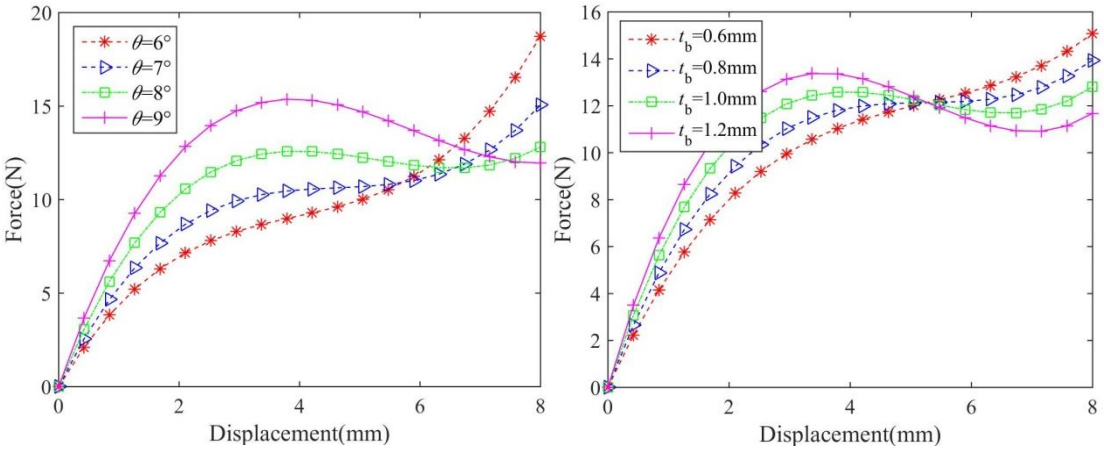

(a) (b)

Fig. 7 The influence of θ, t_b on the constant force properties of the FBCFM (a) θ, (b) t_b

Referring to the Fig. 6 and Fig. 7, some conclusions are summarized as follows: Firstly, in Fig. 6(a), l_2 of the Z-shaped beam varies from 10 to 16 mm gradually with a 2 mm interval. It is seen that the force decreases but constant-force stroke increases as the l_2 increases. In addition, the smaller l_2 is, the greater the influence of l_2 on the output constant force is. Also, with the increasing of l_2, it is better for the FBCFM to exhibit constant force property.

Secondly, in Fig. 6(b), t_z of the Z-shaped beam increases from 0.6 to 1.2 mm with an interval of 0.2 mm. It is seen that the force increases as t_z increases. The relationship between the force and t_z is approximately direct proportional. On the other hand, the change of t_z has nearly no influence on the constant-force stroke.

Thirdly, in Fig. 7(a), the θ of the bi-stable beam varies from 6° to 9° gradually with an interval of 1°. It is observed that the force increases as θ increases. An increase of 1° for θ leads to a force increase of approximately 2 N. The relationship between the force and θ is not directly proportional. Also, as θ increases, the constant-force stroke increases.

Finally, t_b of the bi-stable beam changes from 0.6 to 1.2 mm gradually with a 0.2 mm interval. It is observed that as compared with the other three parameters, t_b has the largest influence on the force. Specifically, the force increases as t_b increases. The larger t_b is, the larger the influence on the force is.

As discussed previously, t_b of the bi-stable beam has the greatest influence on the constant force performance. In addition, from the perspective of machining process, θ of the bi-stable beams is difficult to be guaranteed. Therefore, it is necessary to select the above two parameters to participate in the optimization to exhibit the optimal performance of the FBCFM.

4. Optimization study

It can be seen from section 3 that by changing the value of the architectural parameters, the FBCFM can obtain different force-displacement property. Therefore, within a certain parameter change range, by optimizing and selecting the best value of the parameters, the optimal design of the mechanism can be obtained. The FEA-based optimization of the FBCFM can be implemented by the finite element software Workbench. This method adopts the principle of multi-objective genetic algorithm (MOGA), which can solve the design point composed of different structural parameters and objective parameters, recommend the optimal combination of structural parameters, and obtain the influence relationship of the optimization parameters on the output results. Flowchart of optimization procedure is shown in Fig. 8. In this paper, four independent architectural parameters with their upper and lower limits are selected as optimized parameters as shown in Table II.

Table II Change range of optimized structural parameter

Parameters	Lower limited value	Upper limited value
l_2	12 mm	16 mm
t_z	0.8 mm	1.2 mm
θ	7°	9°
t_b	0.8 mm	1.2 mm

The optimization goal of the FBCFM is to obtain the maximum constant-force stroke by changing the range of selected parameters. To convenience the optimization analysis of the FBCFM, this paper defines a physical quantity as the object parameter: constant-force ratio factor (CSRF). CSRF is defined as the product of input displacement and the size of constant-force travel (original value is 2.2). Therefore, under the condition of constant input displacement, when the CSRF increases, the constant-force stroke will increase accordingly. Considering the actual working environments of the FBCFM, the total deformation maximum (TDM) and equivalent stress maximum (ESM) of the mechanism are selected as objective parameters. The optimization result should maximize the CSRF, TDM and minimize the ESM.

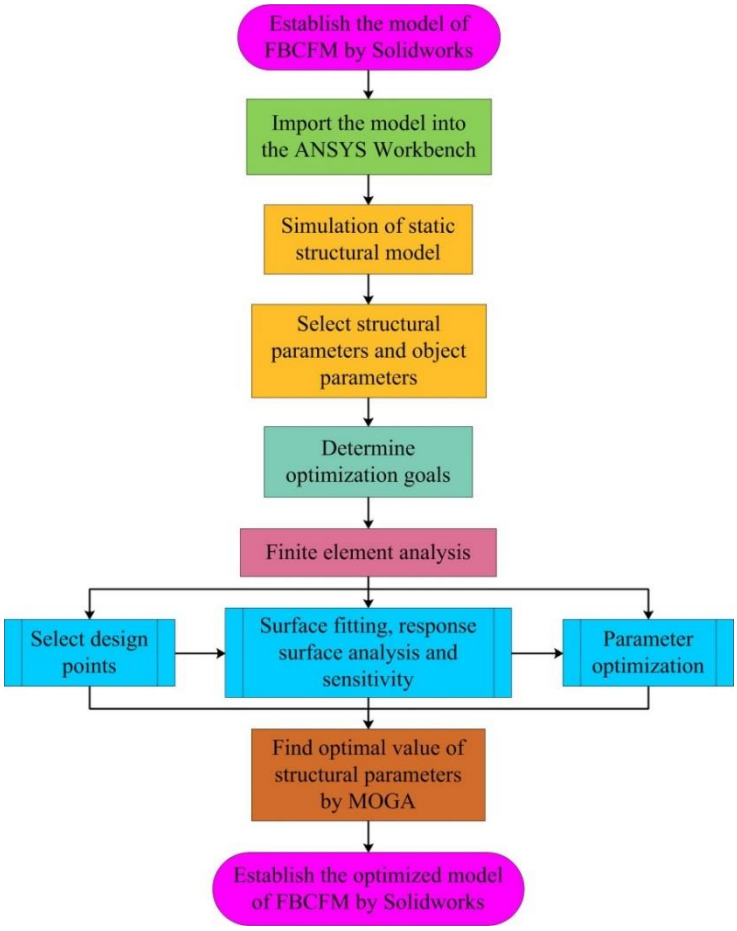

Fig. 8 Flowchart of FEA-based optimization procedure

To achieve the optimization goal, the system will calculate enough design points as a sample reference. The more sample design points collected, the smaller the overall error value of the calculation, which can improve the accuracy of the final optimization. A total of 1004 design points were collected for this optimization, and the sample is shown in Fig. 9. The upper and lower horizontal boundary lines in the figure represent the maximum and minimum values of structural parameters and objective parameters; each curve corresponds to a design point, representing the values of 4 optimized parameters and the corresponding output results. Fig. 10 shows the fitting relationship between the response surface predicted value of the objective parameters and the calculated observed value. It can be seen from Fig. 10 that TDM, ESM and CSRF all exhibit good linear fitting and high accuracy.

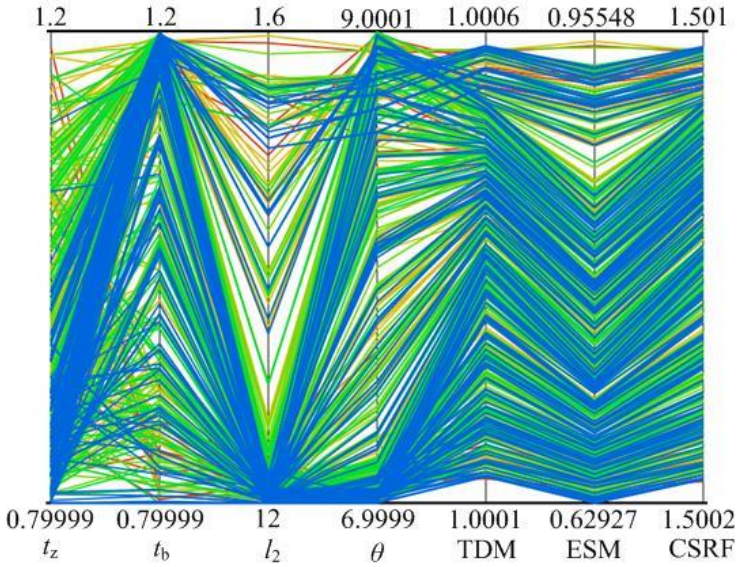

Fig. 9 Design point sampling diagram

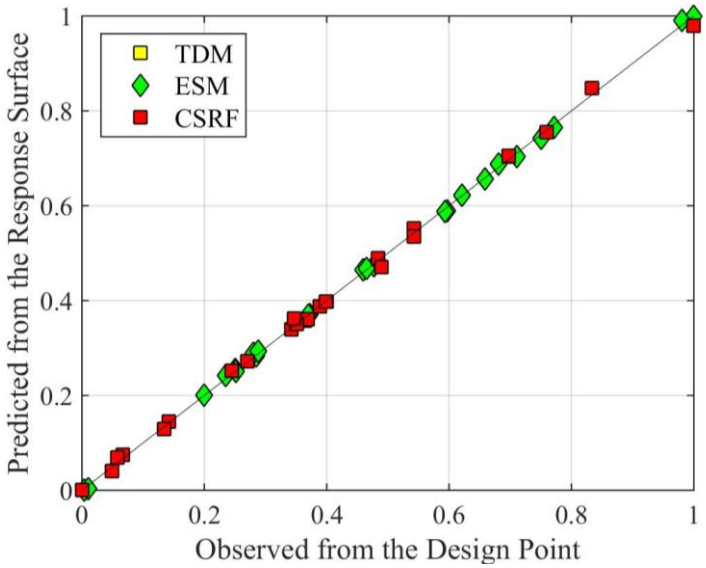

Fig. 10 The fitting curves of predicted and observed values

According to the fitting curve in Fig. 10, the accuracy of the 3D response surface of the objective parameter to the optimized parameter is guaranteed. Through response surface analysis, the relationship between architectural parameters and objective parameters can be obtained. The relationship of different structural parameters to CSRF is mainly analyzed, as shown in Fig. 11. The relationship between the structural parameters and ESM is shown in Fig. 12.

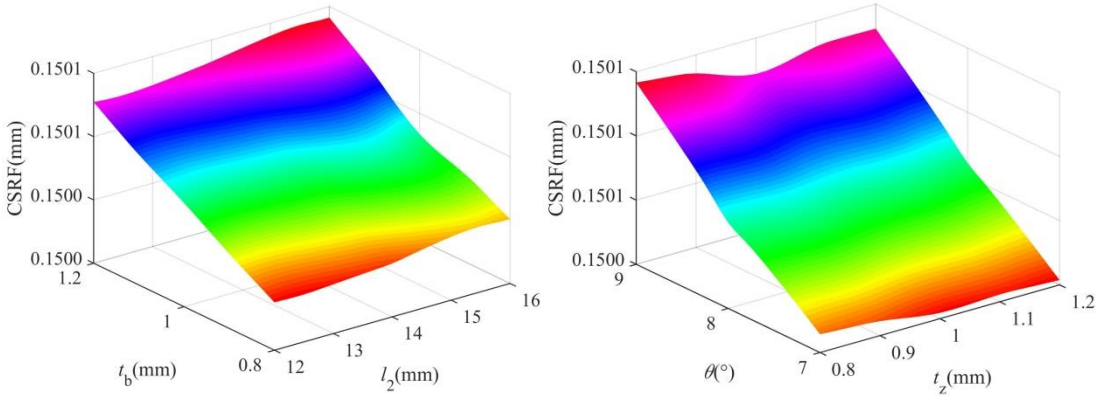

(a) (b)

Fig. 11 The 3D response surface of CSRF to structural parameters (a) l_2 and t_b, (b) t_z and θ

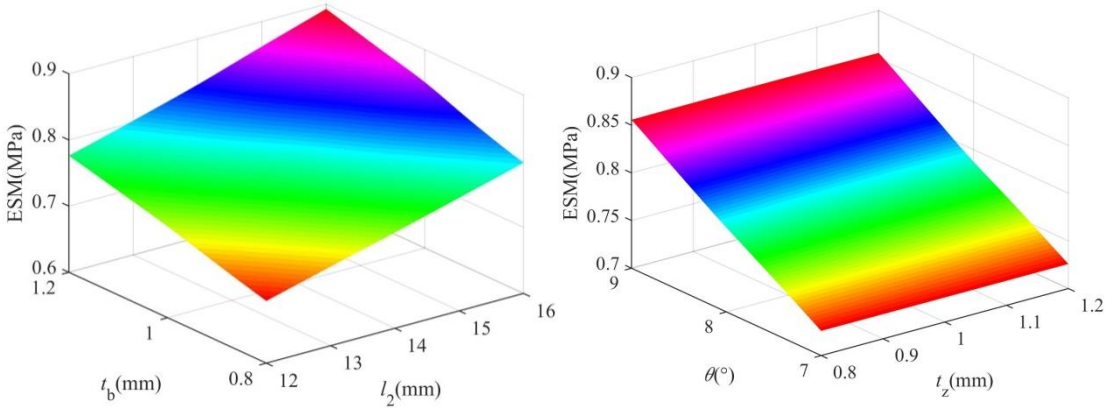

(a) (b)

Fig. 12 The 3D response surface of ESM to structural parameters (a) l_2 and t_b, (b) t_z and θ

According to Fig. 11 and 12, some conclusions are summarized as follows:

1) In Fig. 11, increasing t_b and θ causes CSRF to increase. The two parameters are proportional to CSRF. On the other hand, increasing l_2 and t_z has nearly no influence on the CSRF.

2) In Fig. 12, increasing t_b, l_2 and θ causes ESM to increase. The three parameters are proportional to ESM. On the other hand, increasing t_z has nearly no influence on the ESM.

As discussed previously, t_b and θ of the bi-stable beam has the greatest influence on the CSRF. This is more consistent with the influence of t_b and θ on constant force property in section 3. On the other hand, t_b, l_2, θ and t_z have a good linear fitting relationship to the ESM. The four parameters of the FBCFM are easy to be guaranteed to obtain small ESM.

From 3D response surface analysis, it can be seen that each optimized parameter has a different effect on the objective parameter. In addition, each optimized parameter has a different influence degree on the objective parameter, that is, the influence of individual optimized parameters on the objective parameters is greater than other optimized parameters. The sensitivity of optimized structural parameters to objective parameters is shown in Fig. 13. Individual structural parameter has same effect of influence on CSRF and TDM, and t_b has the greatest effect on the two objective parameters, followed by θ and l_2, and finally t_z; among the effect of each optimized structural parameter on ESM, θ have greatest effect on it, followed by l_2 and t_b, and finally t_z. Therefore, to exhibit the best constant force characteristic of the FBCFM, more attention should be paid on changing of the structural parameters of the bi-stable beam.

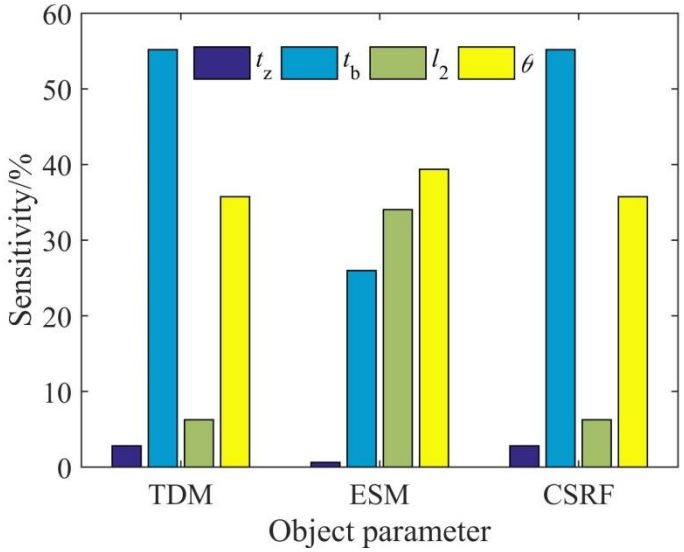

Fig. 13 Sensitivity of structural parameters to objective parameters

Under the 3D response surface and sensitivity of each optimized structural parameter to the object parameter are known, the structural parameters need to be optimized according to the optimization goal. In the optimization module of Workbench, the MOGA can find the optimal solution set on the 3D response surface generated by the structural parameters and object parameters, as shown in the Fig. 14. According to the optimization goal, find the best design candidate points in the optimal solution set, as shown in the Fig. 15.

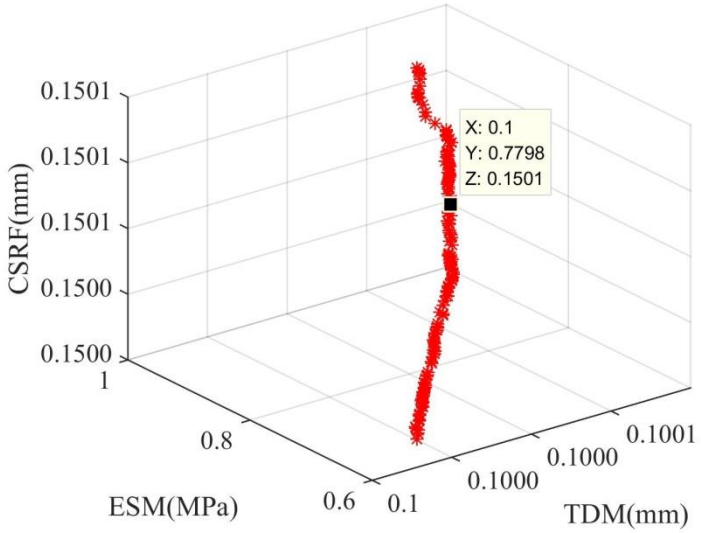

Fig. 14 Optimal solution set of objective parameters

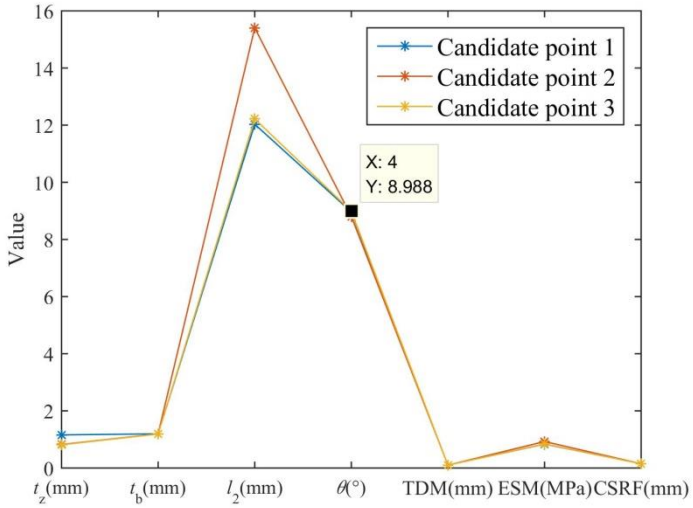

Fig. 15 Optimization candidate points

Through the optimal selection of three candidate points and the best recommendation of the system, Candidate point 2 is utilized as the final value of optimized structural parameters and object parameters. The optimal values of four structural parameters selected in this paper are shown in Table III.

Table III Optimal values of parameters

Optimal values of parameters				
parameters	l_2	t_z	θ	t_b
values	15.40mm	0.82mm	8.80°	1.20mm

The original values are replaced with the optimal values of the four optimized structural parameters, and using SolidWorks software to model. Optimized test prototype is fabricated, and an experiment is set up to verify the feasibility of FEA-based optimization method.

5. Experimental verification

5.1 Experimental setup

An optimized FBCFM prototype are fabricated by a 3D printer (model: 3DP-25-4F) to verify the reliability and feasibility of the FEA-based optimization. The comparison of the original and optimized prototype is shown in the Fig. 16. The adopted material of PLA-ST exhibits good stiffness characteristic, as revealed in previous section 2.4.

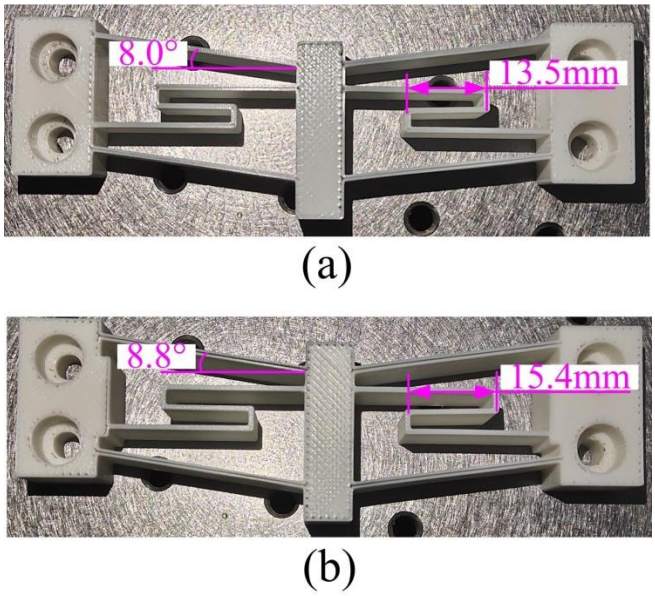

Fig. 16 Comparison of the original and optimized prototype (a) original prototype, (b) optimized prototype

The experimental setup is shown in Fig. 17, including the prototype, voice coil motor, grating ruler, force sensor, motor driver, and industrial control computer. The voice coil motor (model: TMEC100-015-000) is driven by a commercial linear servo amplifier (model: ACJ-055-18) to deliver a nominal travel stroke of 5 mm. One force sensor (model: DS2-XD) with a range of 50 N and a resolution of 0.01 N is mounted at the input end to measure the force of FBCFM, respectively. A grating ruler (model: LaRW1-3D, Fagor Automation) is used to measure the input displacement.

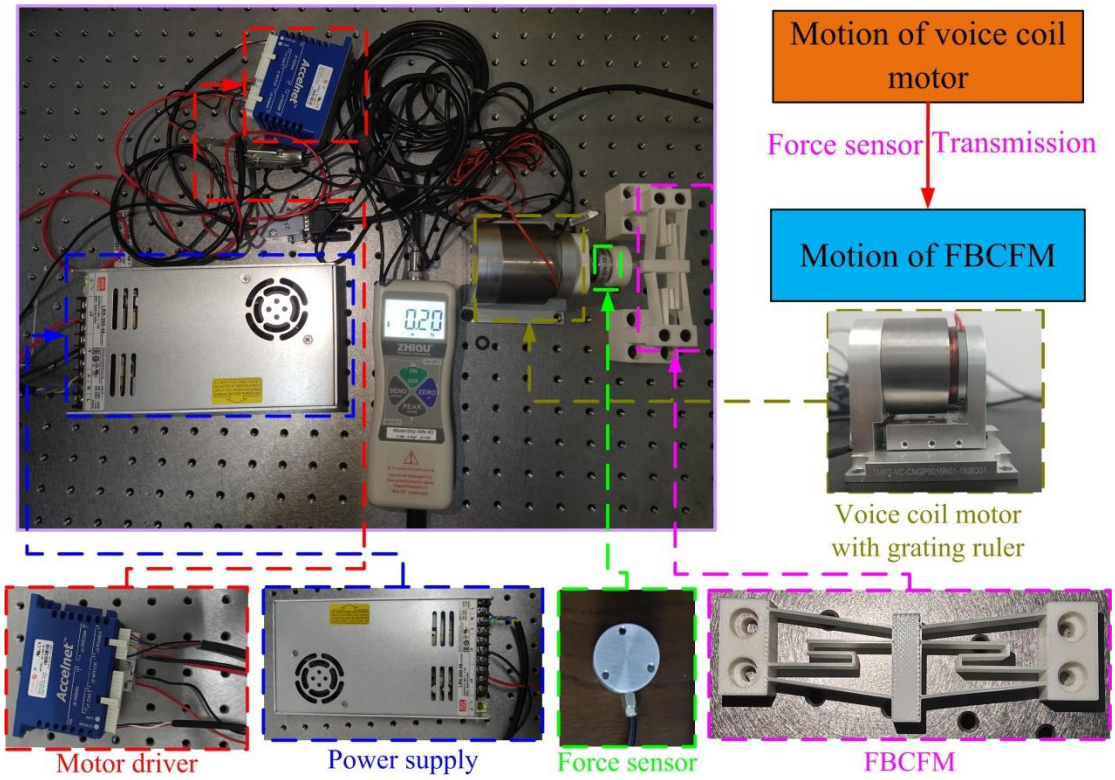

Fig. 17 Experimental setup

5.2 Experimental results

In the experimental test, the displacement-time of the voice coil motor measured by the grating ruler is shown in the Fig. 18. The movement speed of the voice coil motor is 0.5 mm/s. The comparison of multiple experimental results is shown in the Fig. 19. Referring to this Figure, as the number of experimental tests increases, the value of the output force will gradually decrease, and the error will increase. The reason for the error is that due to the limitation of the printing material, with repeated experimental operations, the capability of elastic recovery of the mechanism will be reduced, and it is difficult to form a stable constant force property. In order to make the experimental results more reliable and reduce contingency, the previous three valid test data are collected as a basis.

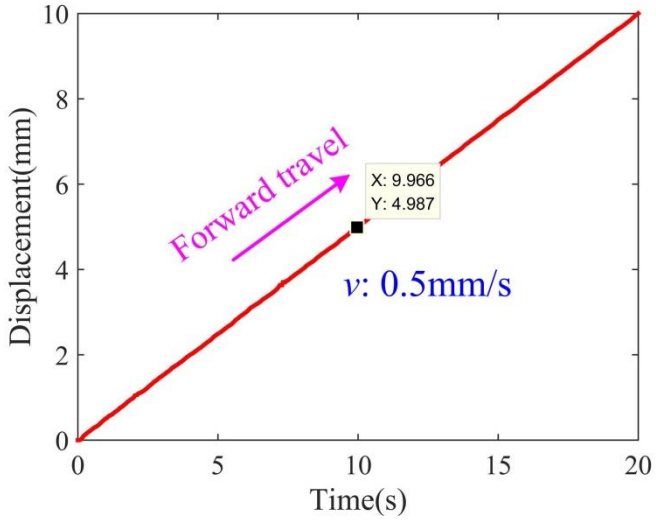

Fig. 18 Displacement-time curve of voice coil motor

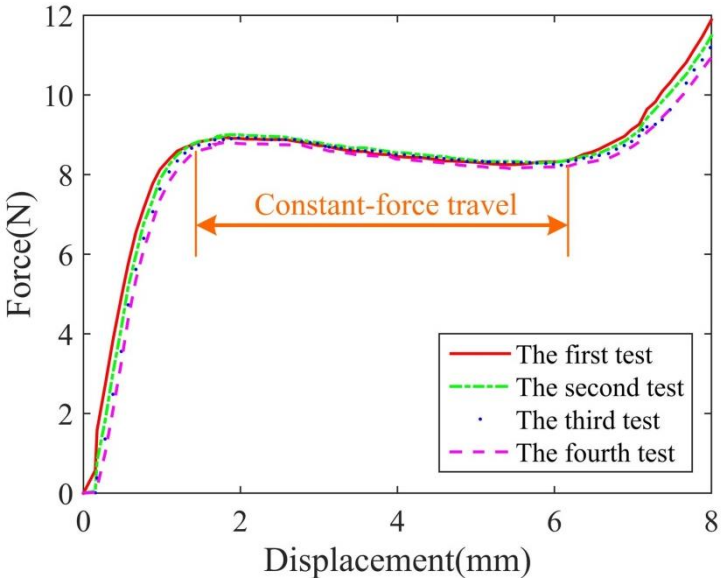

Fig. 19 Comparison of multiple experimental results

The force-displacement properties of the optimized FBCFM are compared with the original FBCFM, and the result is shown in Fig. 20. The optimized FBCFM still has

property of constant force output. The force-displacement curve starts to become flat when the input displacement is approximately 1.5 mm with constant output force approximately 8.5 N, and constant force change range is approximately [8.24, 8.88] N. The constant-force displacement interval is approximately [1.7, 6.2] mm. Compared with the original FBCFM, the constant-force stroke is increased by 2.3 mm. Therefore, the validity and reliability of the FEA-based optimization method are verified. Due to the versatility of the FEA-based optimization, the method is not only applicable to various CFMs derived from the FBCFM, but also other compliant transmission mechanisms by parameter optimization.

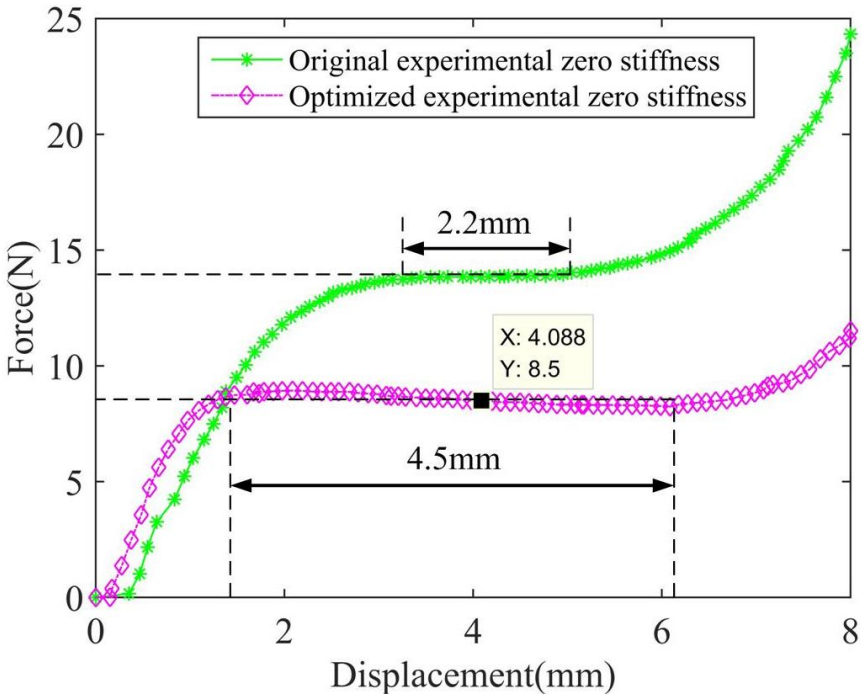

Fig. 20 Comparison of constant force properties based on the original FBCFM and optimized FBCFM

6. Conclusions

This paper proposes a FEA-based optimization method for a typical FBCFM, which can obtain the optimal constant force property of the FBCFM under the optimization goal of a larger constant-force stroke. Firstly, through the design and modeling of the FBCFM combined with Z-shaped beam and the bi-stable beam, the main structural parameters of the FBCFM are obtained. In addition, the influence of each structural parameter on the FBCFM's constant force property is evaluated with MATLAB. Furthermore, the four structural parameters of the FBCFM are selected as optimized parameters, CSRF, TDM and ESM are selected as objective parameters, and the FEA-based optimization method is utilized for optimization of constant force property. Based on the 3D response surface and parametric sensitivity in the optimization process, it is concluded that the sensitive key parameter of the constant force property is t_b. The constant-force stroke of the optimized FBCFM is [1.7, 6.2] mm, the constant output force is 8.5 N, and the constant-force variation is [8.24, 8.88] N. Finally, the validity and reliability of the FEA-based optimization method are verified by

experimental setup. The research results can play a positive role in promoting the research on parametric optimization and application of CFM.

Acknowledgements

This work is supported by Huxiang High Level Talent Project of Hunan Province (Grant No. 2019RS1066), the Project State Key Laboratory of Ultra-precision Machining Technology of Hong Kong Polytechnic University (Project ID：P0033453).

References

[1] Mammano G S, Dragoni E. Mechanical design of buckled beams for low-stiffness elastic suspensions: Theory and application. Journal of Materials: Design and Applications, 2016: 1-11.

[2] Li B K, Hao G B. Nonlinear behaviour design using the kinematic singularity of a general type of double-slider four-bar linkage. Mechanism and Machine Theory, 2018, 129: 106-130.

[3] Zhou J X, Xiao Q Y, Xu D L, Ouyang H J, Li Y L. A novel quasi-zero-stiffness strut and its applications in six-degree-of-freedom vibration isolation platform. Journal of Sound and Vibration, 2017, 394(2): 59-74.

[4] Xie Q Z, Liu S Y, Jiang H X. Design of a passive constant-force mechanism based on a five-bar mechanism. Mechanism and Machine Theory, 2020, 143(103662): 1-12.

[5] Wang J Y, Lan C C. A constant-Force compliant gripper for handling objects of various sizes. Journal of Mechanical Design, 2014, 136(071008): 1-10.

[6] Kuo Y L, Huang S Y, Lan C C, et al. Sensorless Force Control of Automated Grinding/Deburring Using an Adjustable Force Regulation Mechanism. 2019 International Conference on Robotics and Automation (ICRA), 2019: 9489-9495.

[7] Hoetmer K, Kim G W C, Herder J. Negative Stiffness Building Blocks for Statically Balanced Compliant Mechanisms: Design and Testing. Journal of Mechanisms and Robotics, 2010, 2(4): 1-7.

[8] Zhang X Z, Wang G W, Xu Q S. Design, Analysis and Testing of a New Compliant Compound Constant-Force Mechanism. actuators, 2018, 7(4) : 65.

[9] Hao G B, John M, Kwvin C. Simplified modeling and development of a bi-directionally adjustable constant-force compliant gripper. Journal of Mechanical Engineering Science, 2017, 231(11) : 2110-2123.

[10] Liu C H, Hsu M C, Chen T L, Chen Y. Optimal Design of a Compliant Constant-Force Mechanism to Deliver a Nearly Constant Output Force Over a Range of Input Displacements. Soft Robotics, 2020, 7(6): 758-769.

[11] Yong Y K, Fleming A J, Moheimani S O R. A Novel Piezoelectric Strain Sensor for Simultaneous Damping and Tracking Control of a High-Speed Nanopositioner. IEEE/ASME Transactions on Mechatronics, 2013, 18(3): 1113-1121.

[12] Huang H B, Sun D, Su H, et al. Force Sensing and Control in Robot-Assisted Suspended Cell Injection System. Advances in Robotics & Virtual Reality, 2012,

26: 61-88.
[13] Mokrane B, Marcelo G D F, Yann L G, Yassine H, Philippe L. An output feedback LPV control strategy of a nonlinear electrostatic microgripper through a singular implicit modeling. Control Engineering Practice, 2014, 28: 97-111. doi:10.1109/AIM.2009.5229961.
[14] Zhang X Z, Xu Q S. Design and testing of a novel 2-DOF compound constant-force parallel gripper. Precision Engineering, 2019, 56: 53-61.
[15] Li M, Cheng W, Xie R L. Design and experimental validation of a cam-based constant-force compression mechanism with friction considered. Journal of Mechanical Engineering Science, 2019, 233(11): 3873-3887.
[16] Chen G M, Chang H Y, Li G. Design of Constant-Force Compliant Sarrus Mechanism Considering Stiffness Nonlinearity of Compliant Joints. Mechanisms and Machine Science, 2016, 36: 107-116.
[17] Chen F, jiang Du Z, Yang M, Gao F, Dong W, Zhang D. Design and analysis of a three-dimensional bridge-type mechanism based on the stiffness distribution. Precision Engineering, 2018, 51:48–58.
[18] Rommers J, Wijk V V D, Herder J L. A new type of spherical flexure joint based on tetrahedron elements. Precision Engineering, 2021, 71: 130-140.
[19] Yang Y L, Wu G H, Wei Y D. Design, modeling, and control of a monolithic compliant x-y-θ microstage using a double-rocker mechanism. Precision Engineering, 2021, 71: 209-231.
[20] Ding B X, Yang Z X, Xiao X, Zhang G. Design of reconfigurable planar micro-positioning stages based on function modules. IEEE Access, 2019, 7: 15102-15112.
[21] Miao Y B, Zheng J F. Optimization design of compliant constant-force mechanism for apple picking actuator. Computers and Electronics in Agriculture, 2020, 170(105232): 1-7.
[22] Meaders J C, Mattson C A. Optimization of near-constant force springs subject to mating uncertainty. Struct Multidisc Optim, 2010, 4: 1-15.
[23] Ma F L, Chen G M, Wang H T. Large-Stroke Constant-Force Mechanism Utilizing Second Buckling Mode of Flexible Beams: Evaluation Metrics and Design Approach. Journal of Mechanical Design, 2020, 142(103303): 1-7.
[24] Liu Z, Niu F J, Gao H B, Yu H T, Ding L, Li N, Deng Z Q. Design, analysis, and experimental validation of an active constant-force system based on a low-stiffness mechanism. Mechanism and Machine Theory, 2018, 130: 1-26.
[25] Wang D A, Chena J H, Pham H T. A constant-force bistable micromechanism. Sensors and Actuators A: Physical, 2013, 189: 481-487.
[26] Tolman K A, Merrian E G, Howell L L. Compliant constant-force linear-motion mechanism. Mechanism and Machine Theory, 2016, 106: 68-79.
[27] Chen Y H, Lan C C. An Adjustable Constant-Force Mechanism for Adaptive End-Effector Operations. Journal of Mechanical Design, 2012, 134(031005): 1-9.
[28] Jin R Y, Rocco P L, Ghen Y H. Cartesian trajectory planning of space robots using a multi-objective optimization. Aerospace Science and Technology, 2021,

108(106360): 1-11.
[29] Mohammadali G, Bijan S, Ammar A J, Tilok K D, Joshua P. FEA-based optimization of a complete structure of a monolithic z/tip/tilt micromanipulator. Journal of Micro-Bio Robotics, 2020, : 1-18.
[30] Zhou Z F, Gao Y Z, Sun L N, Dong W, Du Z J. A bistable mechanism with linear negative stiffness and large in-plane lateral stiffness: design, modeling and case studies. Mechanical Sciences, 2020, 11(1): 75-89.
[31] Beharic J, Lucas T M, Harnett C K. Analysis of a Compressed Bistable Buckled Beam on a Flexible Support. Journal of Applied Mechanics, 2014, 81(081011): 1-5.
[32] Holst G L, Teichert G H, Jensen B D. Modeling and experiments of buckling modes and deflection of fixed-guided beams in compliant mechanisms. Journal of Mechanical Design, 2011, 133(051002): 1-10.